Supplementary Information

Primary radical ions in irradiated carbonates

Irina S. Tretyakova,[a,b] Vsevolod I. Borovkov,* [a,c]

[a] Voevodsky Institute of Chemical Kinetics and Combustion, SB RAS, 3, Institutskaya str., Novosibirsk, 630090, Russia

[b] Institute of Solid State Chemistry and Mechanochemistry, Kutateladze 18 st., 630090, Novosibirsk, 630090, Russia

[c] Novosibirsk State University, Novosibirsk, 1 Pirogova str., 630090, Russia

* Corresponding author. *E-mail*: borovkov@kinetics.nsc.ru

Section 1. Backgrounds of the method of time-resolved magnetic field effects and the description of the model used to simulate experimental TR MFE curves

The correlation between spin states of electrons, which fill a closed electronic shell in a molecule, is kept after separating these electrons upon ionization of this molecule. In zero magnetic field (see Scheme S1), the spin states of a radical ion pair (RIP) are nearly degenerate thus facilitating equilibration of the populations of all these states due to hyperfine couplings (HFCs) as well as to phase paramagnetic relaxation (see, e.g., refs 1, 2 in the reference list for this section below).

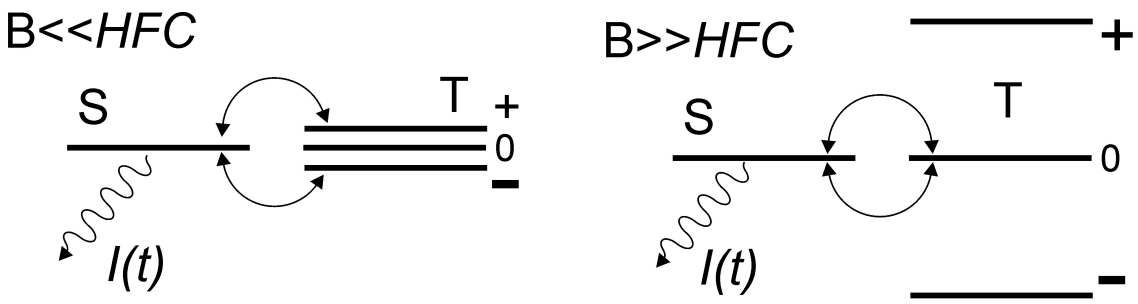

Scheme S1. Singlet (S) and triplets (T) spin sub-levels of a radical ion pair in nearly zero (to the left) and in a strong magnetic field (to the right) upon neglecting spin-spin interactions between the partners. Arrows show S-T mixing due to hyperfine couplings (HFCs) in the radical ions as well as phase paramagnetic relaxation. The wavy line is to emphasize that fluorescence can appear only due to the recombination of the RIP in its singlet state.

In a relatively strong magnetic field, at presence of strong Zeeman interactions of the radicals composing the RIP, the HFC and the paramagnetic relaxation result in mixing of the singlet with, mainly, only one triplet state, T_0. Therefore, if the singlet spin state population of an isolated spin-correlated RIP were monitored via fluorescence from the S-state then, in the absence of spin-lattice

relaxation, the intensity of the recombination fluorescence after singlet-triplet mixing would increase by up to a factor of 2 as a response to turning the magnetic field on.

As the first approximation, the pulsed irradiation of a luminophore solution results in the decay of the recombination fluorescence intensity, *I(t)*, which is proportional to the recombination rate of the RIPs in the singlet spin state:

$$I(t) \propto F(t) \cdot \left[\theta \rho_{SS}(t) + (1-\theta)/4\right], \tag{S1}$$

where $\rho_{ss}(t)$ is the time dependence of the singlet state population of the initially singlet-correlated RIPs. θ is a semiempirical parameter to take into account the fact that in the multiparticle radiation spur only a fraction of recombining RIPs is spin-correlated since some of them are composed of radical ions originating from the different primary ionization events. The second term in the brackets takes account of such spin-uncorrelated RIPs. The possibility of introducing the time-independent parameter θ was previously validated for nonpolar solvents [1, 2]. In particular, this implies that the recombination probability for a RIP does not depend on the RIP's spin state at other things equal.

In this approximation, complexities related to the experimental determining the RIPs' recombination kinetics, *F(t)*, can be avoided with studying the ratio of recombination fluorescence decays, $I_B(t)$ and $I_0(t)$, recorded at the strong and zero magnetic fields. This ratio is referred to as the time-resolved magnetic field effect (TR MFE):

$$\frac{I_B(t)}{I_0(t)} \approx \frac{\theta \cdot \rho_{SS}^B(t) + (1-\theta)/4}{\theta \cdot \rho_{SS}^0(t) + (1-\theta)/4}, \tag{S2}$$

where superscripts *B* and *0* point to strong and zero external magnetic fields, respectively.

The RIP's singlet state population, $\rho_{ss}(t)$, can be evaluated at the magnetic field *B* as previously suggested (see, e.g. [1-3]):

$$\rho_{ss}^B(t) = \frac{1}{4} + \frac{1}{4} exp\left(-\frac{t}{T_1}\right) + \frac{1}{2} exp\left(-\frac{t}{T_2}\right) cos\left(\frac{\Delta g \beta B}{\hbar} \cdot t\right) \cdot G_c^B(t) G_a^B(t), \tag{S3}$$

$$\rho_{ss}^{0}(t) = \frac{1}{4} + \frac{3}{4} exp\left(-\frac{t}{T_0} \right) G_c^0(t)\, G_a^0(t) \quad \text{(S4)}$$

,

where $1/T_{1,2}=1/T_{(a)1,2}+1/T_{(c)1,2}$ are the sums of the longitudinal and phase relaxation rates of the RIP partners, and T_0 is the parameter to describe phase relaxation in a zero magnetic field in the same manner; Δg denotes the difference between the g-values of the RIP partners; β is the Bohr magneton. Subscripts "a" and "c" are to indicate that the parameters relate to radical anion (RA) and radical cation (RC), respectively.

In this work, the contribution of HFC to the spin dynamics was calculated using the semi-classical approximation [3] of functions $G(t)$ as the following in the field units for σ,

$$G^0(t) = \frac{1}{3} \cdot [1 + 2 \cdot (1 - (\gamma\sigma t)^2) \cdot exp[-(\gamma\sigma t)^2 / 2]] \,, \quad \text{(S5)}$$

$$G^B(t) = \exp[-(\gamma\sigma t)^2 / 2)], \quad \text{(S6)}$$

where σ^2 is the second momentum of the radical ion EPR spectrum ($\Delta H_{pp}=2\sigma$), $\gamma=g\beta/\hbar$ is the electron gyromagnetic ratio.

Figure S1 shows some examples of TR MFE curves obtained for a spin-correlated RIP, whose spin state at t=0 is singlet one. In this calculation, it is assumed that the RIP is composed of two radicals, for one of which EPR spectrum width (ΔH_{pp}) is 1 mT and for another one that is 0.2 mT. In this case, if the phase relaxation time (T_2) is long enough then two peaks can be observed on the TR MFE curves. The time position, τ, of the first peak is determined by the larger EPR spectrum width, ΔH_{pp}, and can be estimated as $\tau \approx 18(\text{ns}\cdot\text{mT})/\Delta H_{pp}$.

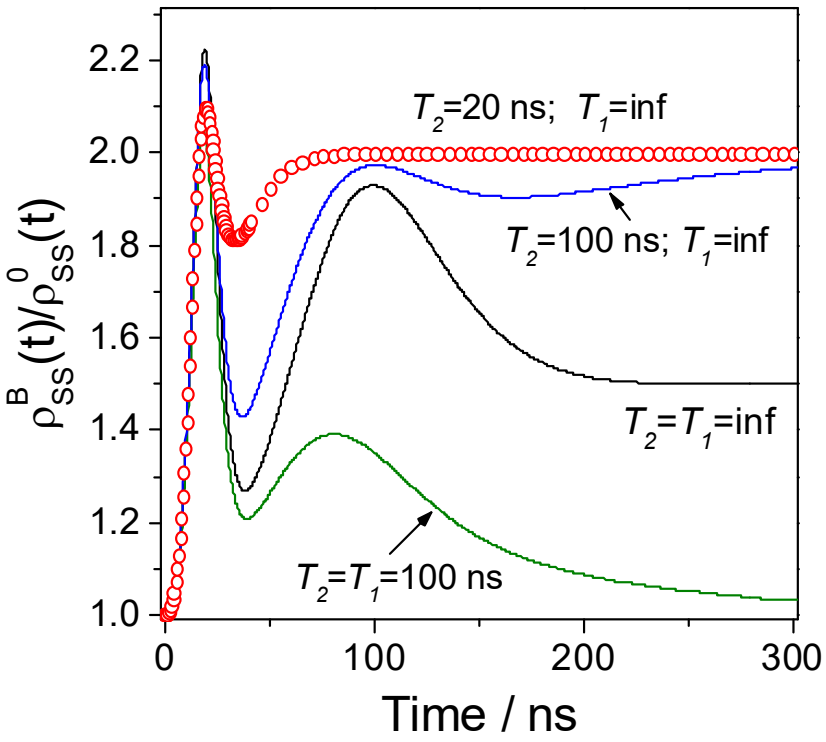

Figure S1. Calculated ratios of the singlet spin populations in a strong and zero magnetic field for a RIP composed of radicals having EPR spectrum width of 1 mT and 0.2 mT to demonstrate effects of HFC as well as of the paramagnetic relaxation. The calculation of the spin dynamics has been performed using eqs. (S2)-(S6) assuming T_0=T_2 and θ=*1*. Particular values of the relaxation times are given in the plots.

Phase paramagnetic relaxation smears the peaks out and flattens the TR MFE curve at the level of θ. Spin-lattice relaxation decreases the ratio magnitude down to the initial value that is equal to 1. Using the terminology of the EPR spectroscopy, the shape of TR MFE curve without gauss-like peaks, similar to those presented in Fig. S1, corresponds to the case of a homogeneously broadened EPR spectrum.

If one of the RIP partners takes part in the electron transfer reaction involving a neutral molecule then this partner is transformed into another radical ion. In this case, Eqs (S3), and (S4) must be modified. Let us consider the reaction, which occurs at the moment t' and results in the

transformation of a reactant, say the primary RC (denoted by *c1* index) into another, secondary RC (*c2*). In this case, later, at $t>t'$, the singlet state population can be calculated as follows [1, 2]:

$$\rho_{ss}^{B}(t,t') = \frac{1}{4} + \frac{1}{4} exp\left(-\frac{t'}{T_1^{(c1)}} \right) exp\left(-\frac{t-t'}{T_1^{(c2)}} \right) + \frac{1}{2} exp\left(-\frac{t'}{T_2^{(c1)}} \right) exp\left(-\frac{t-t'}{T_2^{(c2)}} \right) \times$$
$$\times G_{c1}^{B}(t') G_{c2}^{B}(t-t') G_{a}^{B}(t) \cdot cos\left(\frac{\left(\Delta g_{c1} \cdot t' + \Delta g_{c2} \cdot (t-t') \right) \beta B}{\hbar} \right) \quad \text{(S7)}$$

$$\rho_{ss}^{0}(t,t') = \frac{1}{4} + \frac{3}{4} exp\left(-\frac{t'}{T_0^{(c1)}} \right) exp\left(-\frac{t-t'}{T_0^{(c2)}} \right) G_{c1}^{0}(t') G_{c2}^{0}(t-t') G_{a}^{0}(t) \quad \text{(S8)}$$

If the kinetics of the RC's reaction with bulk molecules can be described correctly using a single reaction time τ then the singlet state population averaged over t' with the exponential distribution at the moment t is of the form:

$$\rho_{ss}(t) = exp(-t/\tau) \cdot \rho_{ss}(t,t) + \frac{1}{\tau} \cdot \int_0^t exp(-t'/\tau) \rho_{ss}(t,t') dt' . \quad \text{(S9)}$$

Eq. (S9) corresponds to the case when the recombination of both types of RIPs, composed of the luminophore RA and either primary or secondary RCs, contributes to the fluorescence equally.

If any radical ion participates in a non-correlated degenerate electron exchange (DEE), one should further modify the above expression to take into account a random change in the projections of nuclear spins in the radical. According to ref. 3, for DEE involving RC, the $G^{B,0}{}_{c}(t)$ functions in Eqs. (S3), (S4) should be substituted for the functions $\Gamma^{B,0}{}_{c}(t)$ determined, at corresponding value of magnetic field (strong or zero), by the equation

$$\Gamma_c(t) = \sum_{n=1}^{n=\infty} G_c^{(n)}(t) \quad \text{(S10)}$$

where $G_c^{(n)}(t) = \tau^{-1} \cdot \int_0^t G_c^{(1)}(t') \cdot G_c^{(n-1)}(t-t')\ dt'$ is the term corresponding to the contribution of the random realization of (n-1) acts of self-exchange by the time t, τ is the mean time between electron jumps, and $G_c^{(1)}(t) = G_c(t) \cdot \exp(-t/\tau)$.

Figure S2a shows the effect of the DEE reaction on the TR MFE curve as calculated using Eqs. (S2-S4), (S10). Similarly to the conventional EPR, the exchange results in narrowing the EPR spectrum width that manifests itself as disappearing the corresponding peak.

In the case when several RIPs contribute to the recombination fluorescence intensity simultaneously then both the nominator and denominator in Eq. (S2) should include corresponding contributions of each pair. Note that the parameter θ should be the same for these contributions since this is determined by the primary radiation spur structure.

The difference in the *g*-values of the RIP's partners results in so-called Δg-beats in the recombination fluorescence.[1] The frequency of these beats increases linearly with external magnetic field according to Eq (S3). Note that the Δg-beats can only be observed within the time range limited by the time position of the first peak determined by HFC in the partner with larger EPR spectrum width (Fig. S2b). Another important point is that, at early time, the significant difference in the g-values results in a decrease in the TR MFE curve below 1, while HFC couplings results in an average increase in the curve.

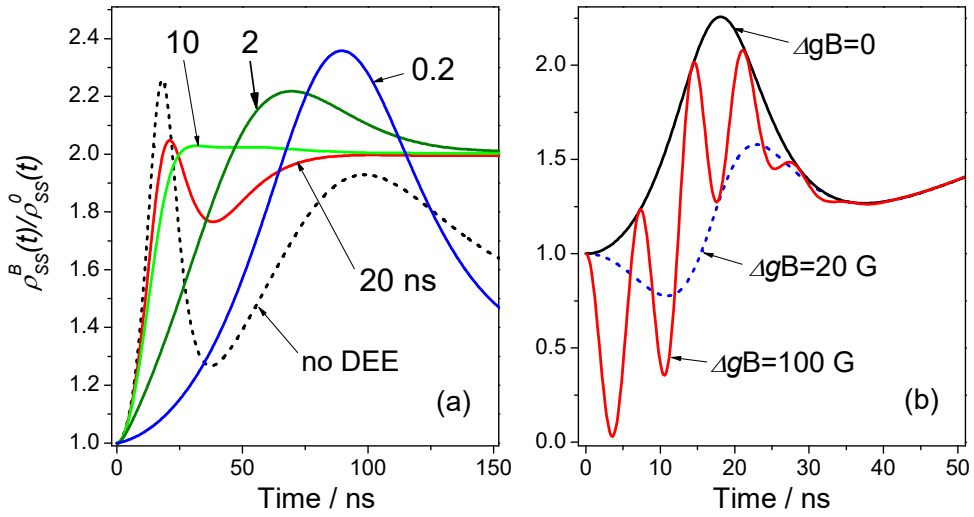

Figure S2. Calculated ratios of the singlet spin populations in a strong and zero magnetic fields for a RIP composed of radicals having EPR spectrum width of 1 mT and 0.2 mT neglecting paramagnetic relaxation. Plot (a): the radical, which has larger ΔH_{pp} value, participates in degenerate electron exchange with the exchange time, τ, whose value is indicated in the plot in nanoseconds; Plot (b): the radical with the larger

ΔH_{pp} value has the g-value, which is different from the g-value of its counter ion without a spectral exchange. The frequency of Δg-beats is determined by the product $\Delta g \cdot B$ (see Eq *S3*) that is given in the plot.

References to Section 1

1. V. A. Bagryansky, V. I. Borovkov and Y. N. Molin, Quantum beats in radical pairs, *Russ. Chem. Rev*., 2007, **76**, 493-506.

2. V. Borovkov, D. Stass, V. Bagryansky and Y. Molin, Study of spin-correlated radical ion pairs in irradiated solutions by optically detected epr and related techniques. In: *Applications of EPR in radiation research*, Ed. by Lund, A. and Shiotani, M.; Springer International Publishing: Cham, Switzerland, **2014**, 629–663.

3. K. Schulten and P. G. Wolynes, Semiclassical description of electron spin motion in radicals including the effect of electron hopping, *J. Chem. Phys*. 1978, **68**, 3292−3297.

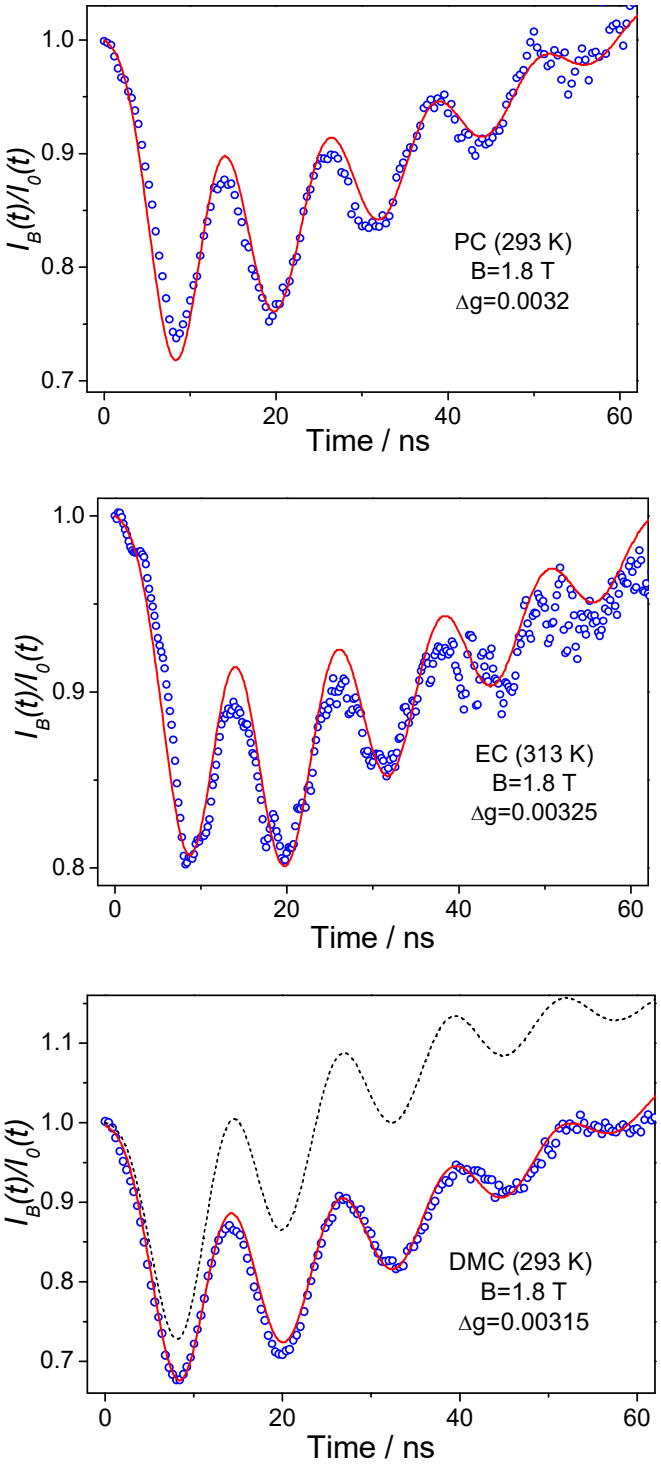

Figure S3. Experimental (circles) and calculated (lines) curves TR MFE, $I_B(t)/I_0(t)$, for solution 0.5 mM *p*-TP-d_{14} in ethylene carbonate (EC), propylene carbonate (PC), and dimethyl carbonate (DMC). The calculation of the spin dynamics has been performed using Eqs. (S2)-(S6) at ΔH_{pp}=0.007 mT and ΔH_{pp}=0.006 mT for anion and cation, respectively, and θ = 0.12 (EC), 0.18 (PC), and 0.21 (DMC). For all the curves, phase relaxation time at B = 0 was T_0 = 100±15 ns, phase relaxation time at B = 1.8 T was T_2 = 23±3 ns, T_1 = 300 ns (this parameter was estimated with a low accuracy). The ratio T_0/T_2 ≈ 4-5 indicates the most valuable contribution to the paramagnetic relaxation rate at B = 1.8 T to be the modulation of the *g*-tensor anisotropy by rotation. Short-dashed line for DMC shows the simulation at $T_0 = T_2$.

Section 2. Quantum chemical calculations

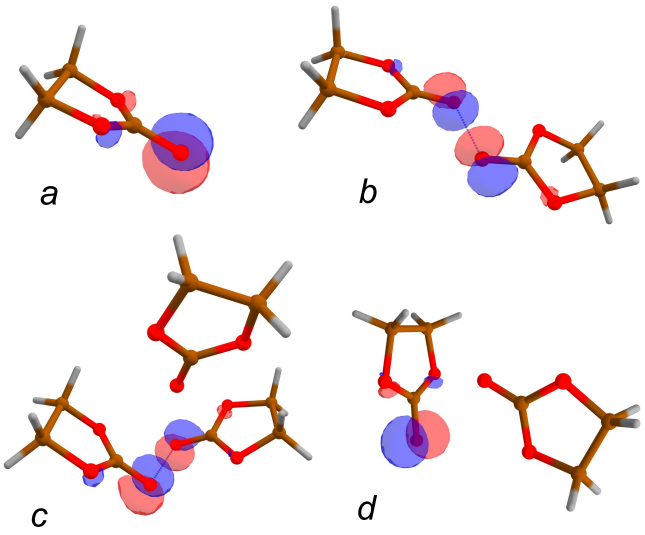

Figure S4. Estimated SOMO density distribution (GAMESS, DFT, CAMB3LYP/6-31+G*, SOLVENT=H2O) for (a) $EC^{+\bullet}$; (b) complex of $EC^{+\bullet}$ with one molecule ($EC_2^{+\bullet}$); (c) complex of $EC^{+\bullet}$ with two molecules ($EC_3^{+\bullet}$); (d) structure of $EC_2^{+\bullet}$ complex, in which the spin density is localized on one particle.

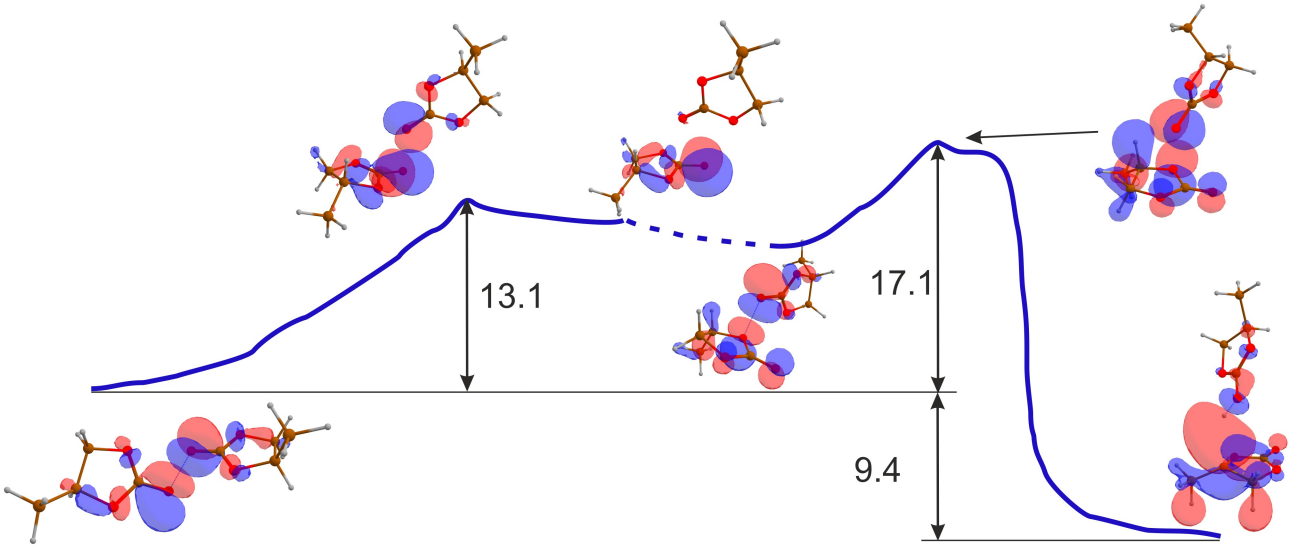

Figure S5. PES profile intermolecular proton transfer reaction within a dimeric radical cation $(PC)_2^{+\bullet}$ (GAMESS, DFT, PBE0/6-31+G*, SOLVENT=DMSO). The dashed line indicates the approximate transition path along the profiles. The energy differences are given in kcal/mol.

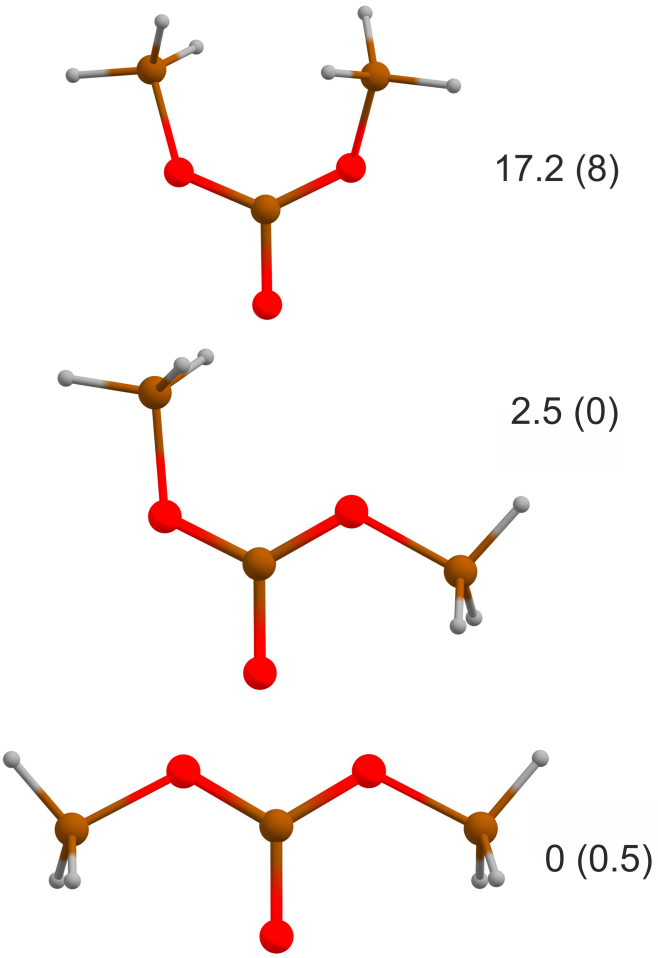

Figure S6. Conformations of the DMC neutral molecule GAMESS, DFT, PBE0/6-31+G*, in gas). The energies of the conformers are given relative to the lowest in energy conformation in kcal/mol. For DMC radical cation, the geometry of corresponding conformations is very close to those shown in the plot. The relative energy of the radical cation conformations is given in parentheses.

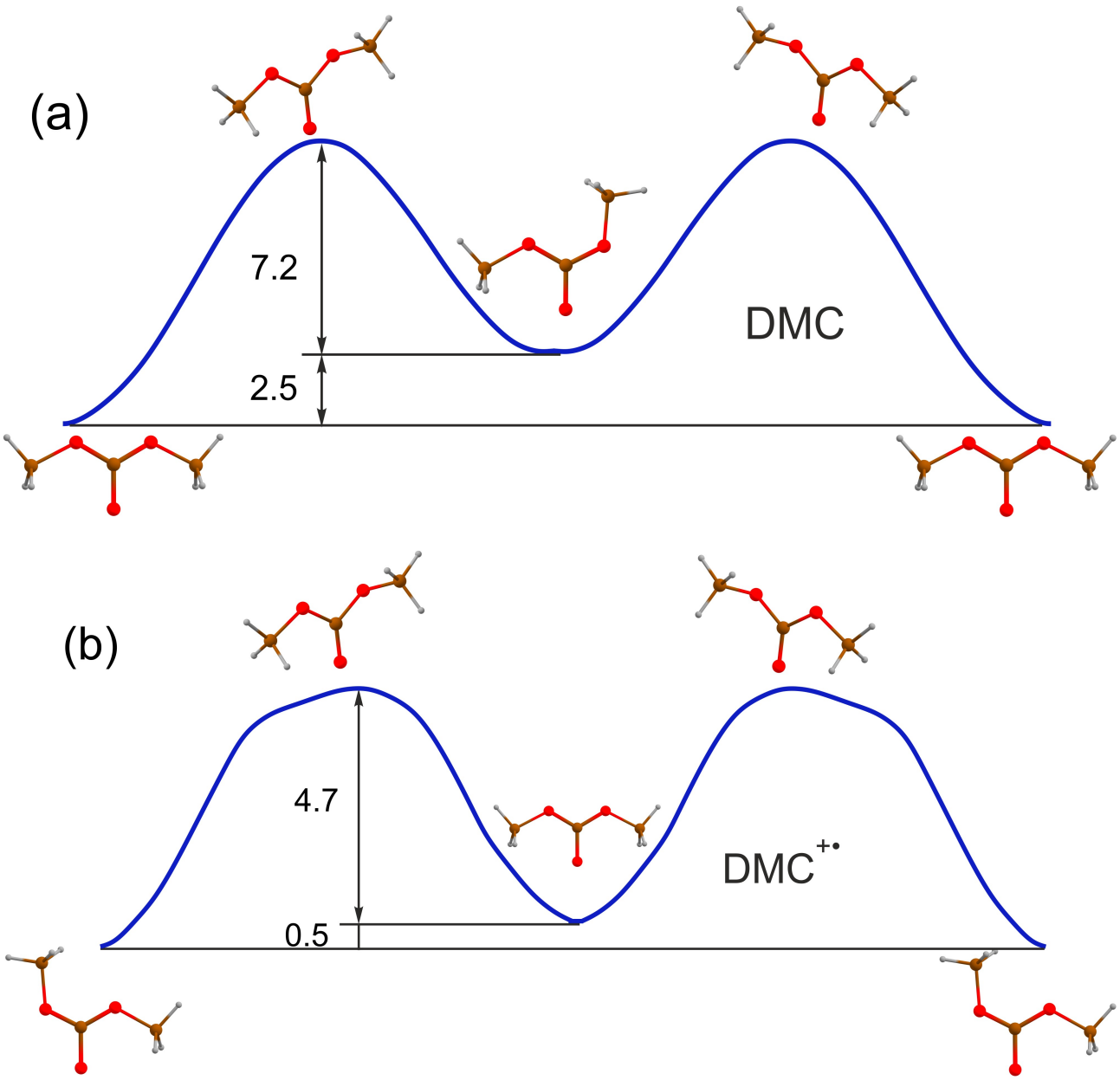

Figure S7. The PES profile for conformational transition of DMC neutral molecule (a) and radical cation (b) for the rotation of only one methoxy group (GAMESS, DFT, PBE0/6-31+G*, SOLVENT=TOLUENE). The energy differences are given in kcal/mol.

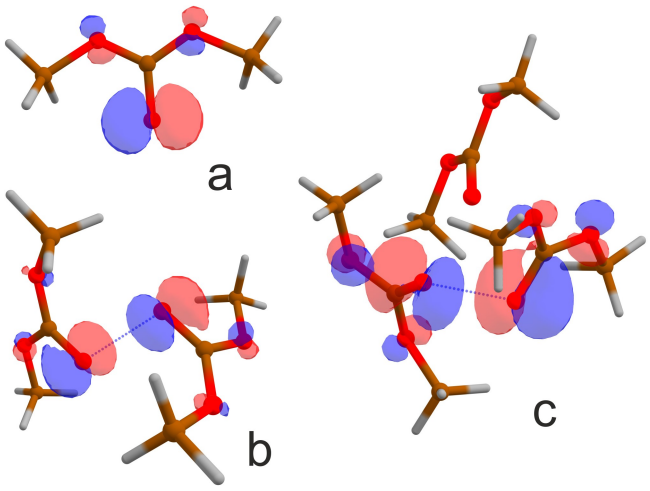

Figure S8. Estimated SOMO density distribution (GAMESS, DFT, CAMB3LYP/6-31+G*, SOLVENT=TOLUENE) for (a) the radical cation of DMC in the geometry of neutral molecule; (b) the complex composed of RC and one molecule ($DMC_2^{+\bullet}$); (c) the complex with two molecules in their ground state ($DMC_3^{+\bullet}$).

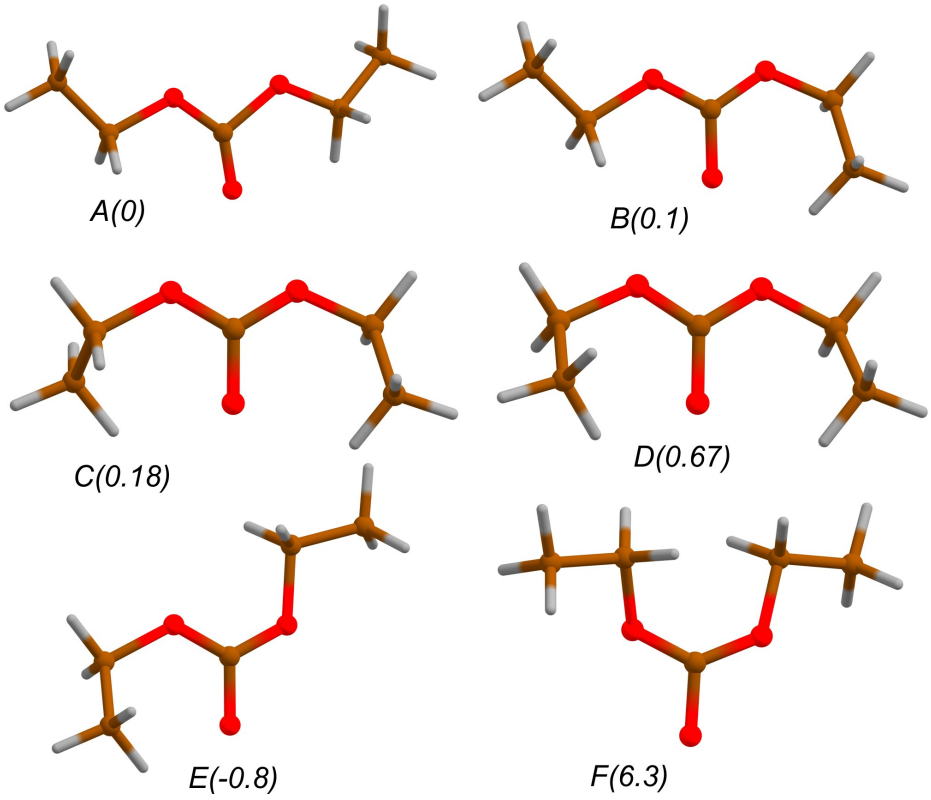

Figure S9. Conformations of the DEC radical cation (GAMESS, DFT, PBE0/6-31+G*, in gas). The energies of the conformers are given in kcal/mol relative to the conformation ***A***. Note that the conformation *E* is lower in energy as compared to *A* but the probability to ionize a molecule in the conformation *E* is very low.

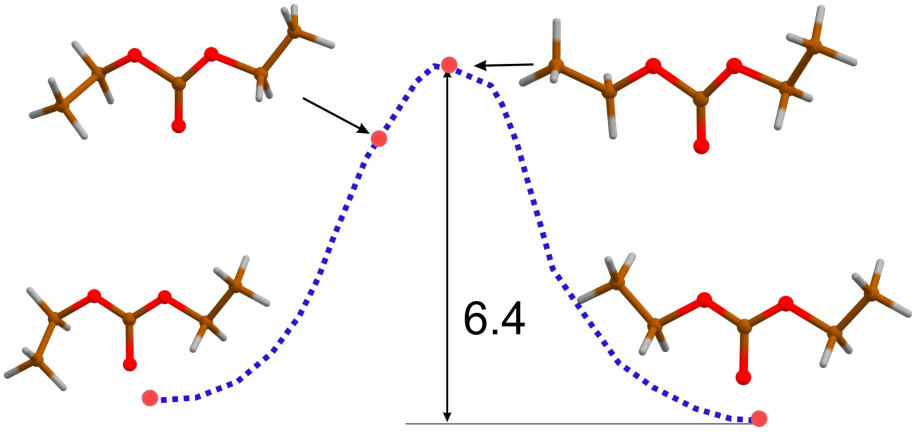

Figure S10. Red points show positions on the PES profile for conformational transition of DEC radical cation between the conformations ***B*** (to the left) and ***A*** (to the right) (GAMESS, DFT, PBE0/6-31+G*, SOLVENT=TOLUENE). The dashed line is given as an eye guide to indicate an *approximate* reaction path.

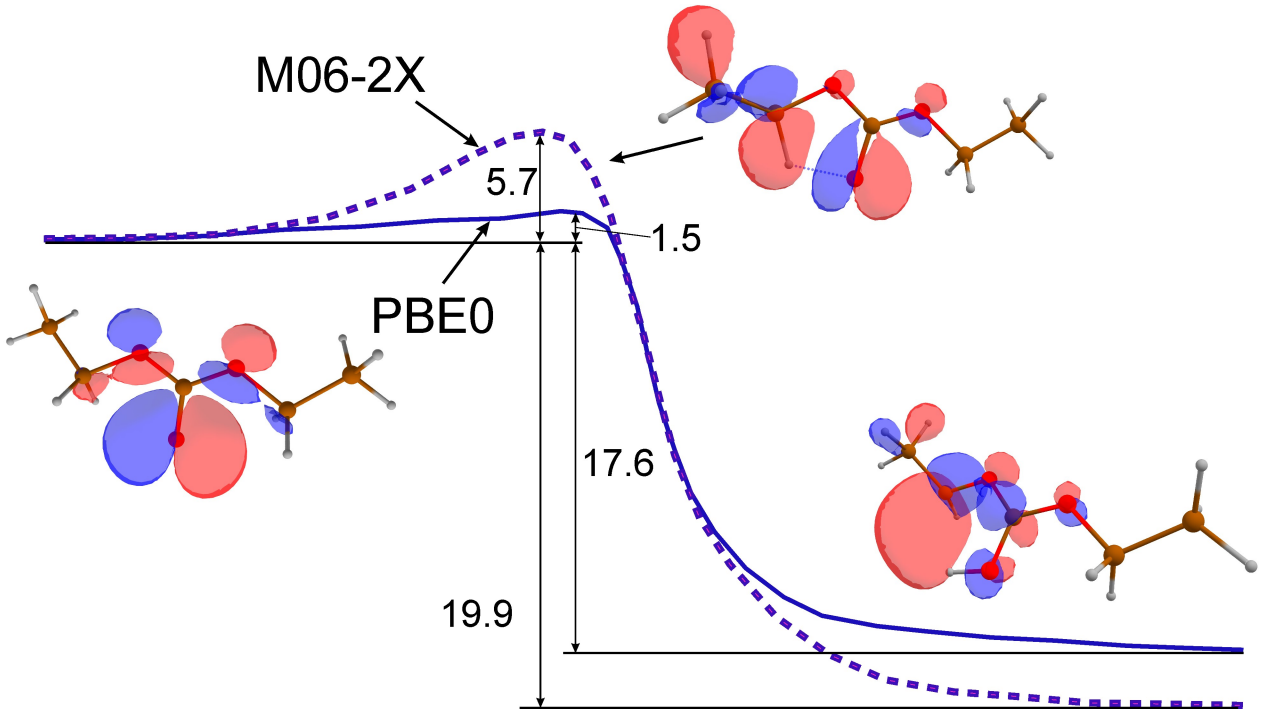

Figure S11. Calculated PES profile for intramolecular proton transfer reaction within radical cation $DEC^{+\bullet}$ in the conformation **B** (see Fig. S9) using functional PBE0 (solid line) or M06-2X (dashed line) (GAMESS, DFT, basis set 6-31+G*, SOLVENT=TOLUENE). The energy differences in kcal/mol are given.

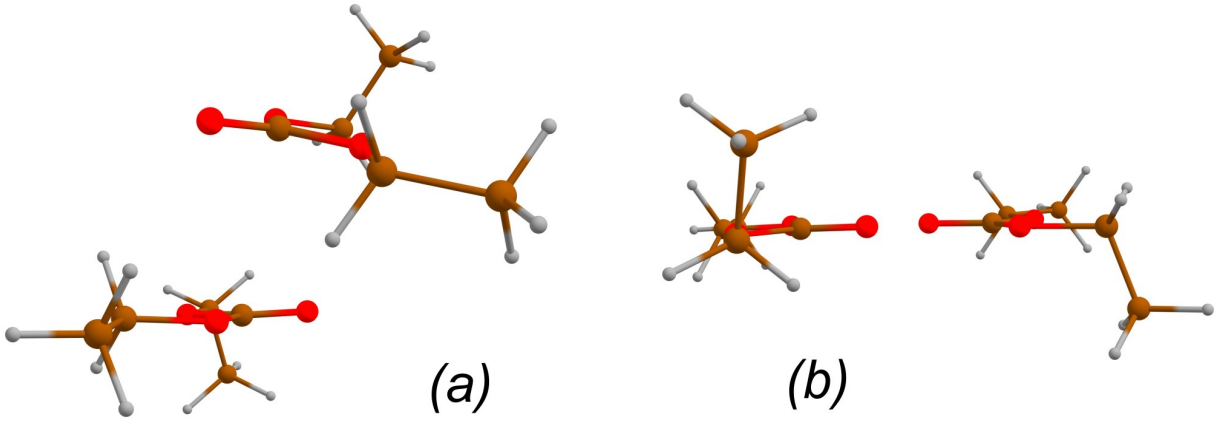

Figure S12. Optimized geometries of (a) $(DEC)_2$; (b) $(DEC)_2^{+\bullet}$. GAMESS, DFT, CAMB3LYP/6-31+G*, PCM.

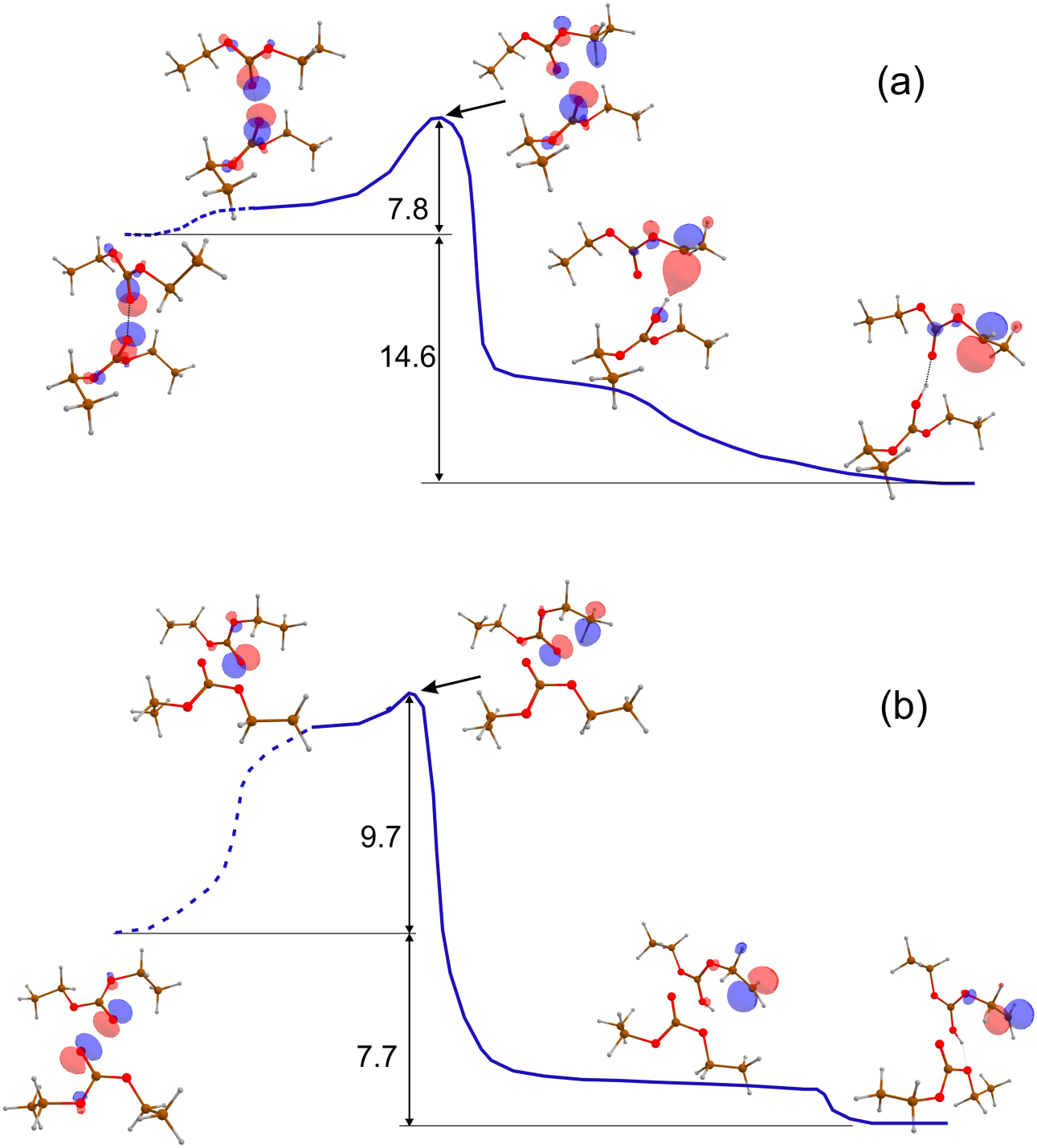

Figure S13. Calculated PES profile for intermolecular (a) and intramolecular (b) proton transfer reaction within a dimeric radical cation $(DEC)_2^{+\bullet}$ (GAMESS, DFT, PBE0/6-31+G*, SOLVENT=TOLUENE). The dashed lines indicate the *approximate transition path* along the profiles. The energy differences are given in kcal/mol.

Table S1. Estimated values of electron detachment energy in gas phase (adiabatic), *DE*; solvation energy, *P* (GAMESS, DFT, CAMB3LYP/6-31+G*, PCM);[a] the isotropic *g*-factors; some HFC constants with protons (averaged over methyl group rotation); ΔH_{pp} values for EPR spectrum of radical anions of studied carbonates and their dimers (ORCA, DFT, PBE0/6-31+G*, CPCM). The solvent used in calculations is indicated in parentheses.

	DE, eV	*P*, eV	*g*	HFC constants, mT; (ΔH_{pp})
$DEC^{-\bullet}$ [b]	-1.53	1.78 (TOLUENE)	2.0028	a(2H) = 0.01; a(2H) = -0.1 a(3H) = 0.10; a(3H) = 0.06 (ΔH_{pp} = 0.25)
$DEC_2^{-\bullet}$	-1.1	1.27 (TOLUENE)	2.0028	a(2H) = 0.05; a(2H) = -0.02; a(6H) = 0.03; a($2H^c$) = 0.02; (ΔH_{pp} = 0.11)
$EC^{-\bullet}$	-1.11	3.05 (H2O)	2.0028	a(2H) = -0.10; a(2H) = 0.14 (ΔH_{pp} = 0.24)
$EC_2^{-\bullet}$	-1.21	3.29 (H2O)	-	a(2H) = 0.13; a(2H) = -0.11; a($2H^c$) = - 0.02 (ΔH_{pp} = 0.24)
$PC^{-\bullet}$	-0.95	2.79 (DMSO)	2.0028	a(3H) = 0.05; a(2H) = 0.06; a(1H) = -0.07 (ΔH_{pp} = 0.14)
$PC_2^{-\bullet}$	-0.46	2.42 (DMSO)	-	a(1H) = 0.33; a(2H) = - 0.10; a($1H^c$) = 0.03; a($3H^c$) = - 0.04 (ΔH_{pp} = 0.37)
$DMC^{-\bullet}$	-1.26	1.59 (TOLUENE)	2.0028	a(3H) = 0.03; a(3H) = 0.02

				(ΔH_{pp} = 0.06)
$DMC_2^{-\bullet}$	-1.08	1.52 (TOLUENE)	2.0028	a(6H) = 0.03; a(3H[c]) = -0.02 (ΔH_{pp} = 0.08)
p-$TP^{-\bullet}$	0.12	1.75 (DMSO) 1.76 (H2O)	2.0026	($\Delta H_{pp} \approx$ 0.069 mT [d])
$DMAT^{-\bullet}$	-0.03	1.66 (DMSO) 1.68 (H2O)	2.0025	($\Delta H_{pp} \approx$ 0.74 mT [e])

[a] Calculated as the difference between the energies of the ground state of radical anion in the gas phase and continuous medium.

[b] The values are given for radical anion in the conformation ***D*** used as an example.

[c] These HFC constants are due to a spin density delocalization to neighboring molecule.

[d] Based on the experimental HFC constants values.[4, 5]

[e] Experimental value.[6]

Table S2. Estimated values of neutralization energy,[a] E_{neutr} (adiabatic); solvation energy, P (GAMESS, DFT, CAMB3LYP/6-31+G*, PCM); the isotropic values of the *g*-factors; HFC constants with protons, and ΔH_{pp} values for EPR spectrum of radical cations of studied carbonates and their aggregates (ORCA, DFT, PBE0/6-31+G*, CPCM). In parentheses, the solvent used is indicated.

	E_{neutr}, eV (gas)	P, eV	*g*-factor	HFC constants, mT
$DEC^{+\bullet}$	10.14	1.24 (TOLUENE)	2.0067[b]	a(3H) = 0.06; a(3H) = 1.4; a(2H) = 12; a(2H) = 0.86 (ΔH_{pp} = 17.2)
$DEC_2^{+\bullet}$	8.97	0.97 (TOLUENE)	2.0052	a(6H) = -0.01; a(9H) = 0.01; a(2H) = 0.06; (ΔHpp = 0.09)
$EC^{+\bullet}$	10.62	2.50 (H2O)	2.0113	a(4H) = 0.14 (ΔH_{pp} = 0.28)
$EC_2^{+\bullet}$	9.34	2.06 (H2O)	2.0054	a(4H) = 0.04; a(4H) = 0.05; (ΔH_{pp} = 0.12)
$EC_3^{+\bullet}$	9.15	2.01 (H2O)	2.0058	a(4H) = 0.06; a(4H) = 0.08 (ΔH_{pp} = 0.20)
$DMC^{+\bullet}$	10.49	1.36 (TOLUENE)	2.0110	a(6H) = -0.02 (ΔH_{pp} = 0.05)
$DMC_2^{+\bullet}$ [c]	9.64	1.14 (TOLUENE)	2.0062	a(6H) = 0.02; a(6H) = 0.08 (ΔH_{pp} = 0.21)
$DMC_2^{+\bullet}$ [d]	9.04	1.06 (TOLUENE)	2.0052	a(6H) = 0.03; a(6H) = -0.01 (ΔH_{pp} = 0.09)
$DMC_3^{+\bullet}$ [c]	9.44	1.08	2.0062	a(6H) = 0.02; a(6H) = 0.04,

		(TOLUENE)		(ΔH_{pp} = 0.1)
$PC^{+\bullet}$	10.45	2.36 (DMSO)	2.0115	a(3H) = 0.09; a(2H) = 0.18; a(1H) = -0.02; (ΔH_{pp} = 0.3)
$PC_2^{+\bullet}$	9.22	1.93 (DMSO)	2.0054	a(2H) = 0.04; a(2H) = 0.03; a(1H) = 0.09; (ΔH_{pp} = 0.11)
$PC_3^{+\bullet}$	9.03	1.84 (DMSO)	2.0058	a(1H) = 0.19; a(2H) = 0.06; a(1H) = -0.01; a(2H) = 0.08, a(3H) = 0.01; (ΔH_{pp} = 0.24)
p-$TP^{+\bullet}$	7.53 [e]	0.98 (TOLUENE) 1.66 (DMSO) 1.68 (H2O)	2.0025 [f]	($\Delta H_{pp} \approx$ 0.075 mT [f])
$DMAT^{+\bullet}$	6.61	0.99 (TOLUENE) 1.71 (DMSO) 1.73 (H2O)	2.0029	($\Delta H_{pp} \approx$ 2.7 mT [g])

[a] The value is calculated as the difference between the energies of the ground state of a radical cation and the ground state of the same system with added electron without changes in the particles' conformation;

[b] The value is given for the conformation ***A***, because for other conformations, in the case of calculation with the dispersed correction in the ORCA program, intramolecular proton transfer occurs during optimization. Note that in the conformation ***A***, there is a significant spin density on two H atoms that correlates with that two C-H bonds in one of the ethyl fragments are lengthened to 0.111 nm and 0.115 nm;

[c] The values are given for the complex composed of particles in the conformation of the ground state of neutral DMC molecule;

[d] The values are given for the complex composed of particles in the conformation of the ground state of DMC radical cation.

[e] The calculated vertical value of the ionization potential for *p*-TP was 7.40 eV (B3LYP) or 7.81 eV (CAMB3LYP). The experimental value is about of 7.8 eV.[7]

[f] Based on the experimental data[5, 8]

[g] Experimental value.[6]

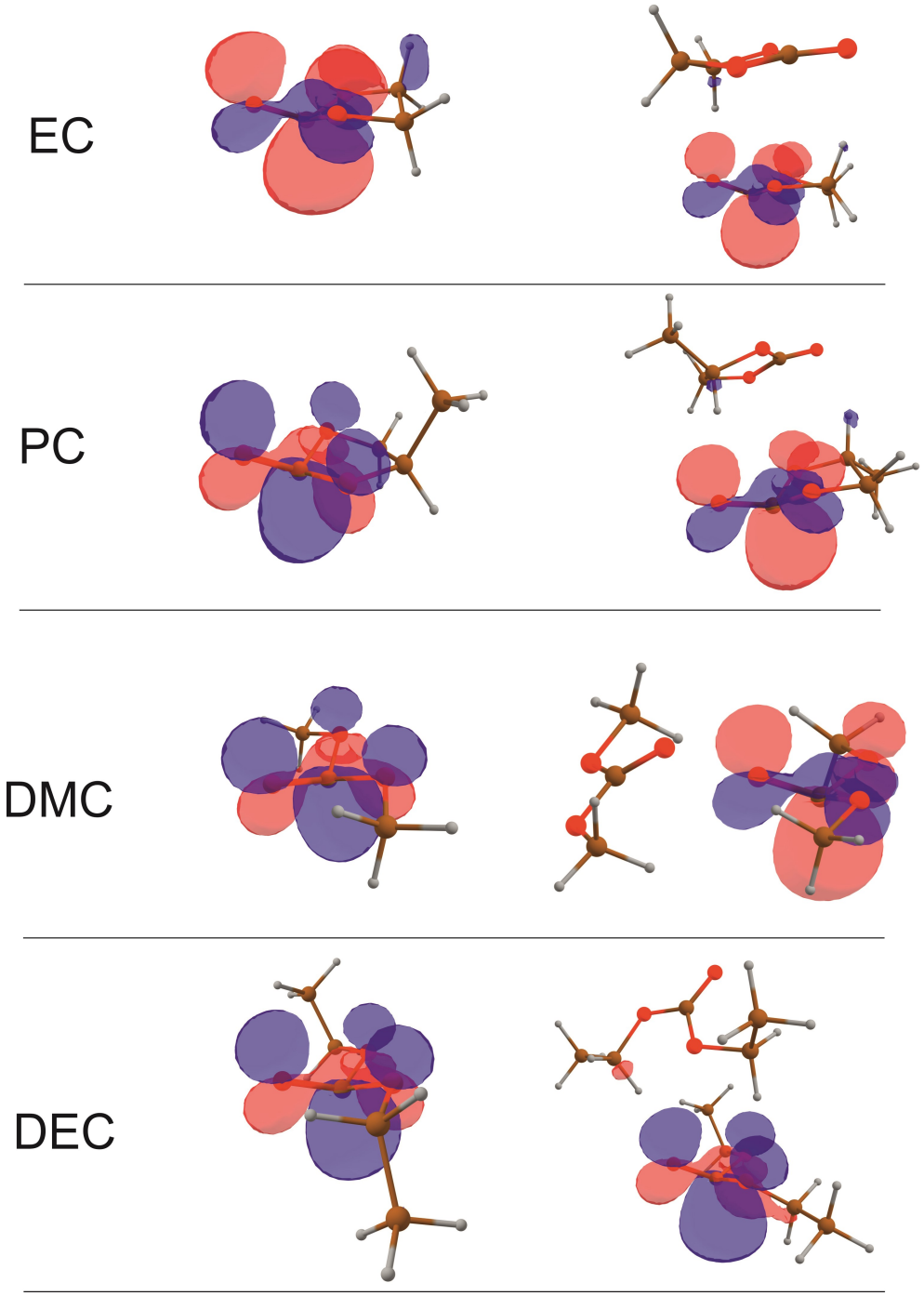

Figure S14. Estimated density distribution SOMO for isolated radical anions (structures to the left) and dimeric structures of the radical anions (structures to the right) of studied carbonates in a medium with the polarity close to the polarity of corresponding carbonate (GAMESS, DFT, CAMB3LYP/6-31+G*, PCM)

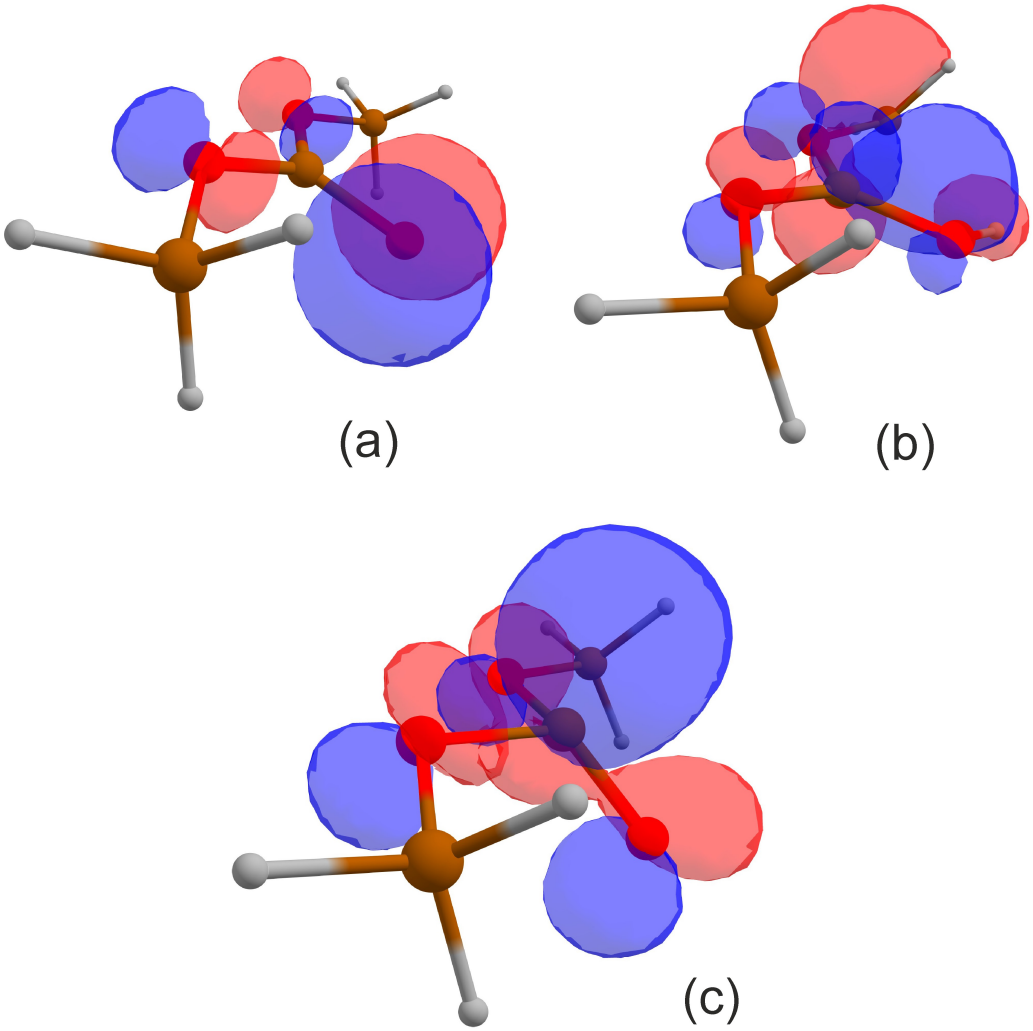

Figure S15. Estimated density distribution SOMO for isolated radical cation before (a) and after (b) proton transfer and anion radical of DMC (GAMESS, DFT, CAMB3LYP/6-31+G*, SOLVENT=TOLUENE).

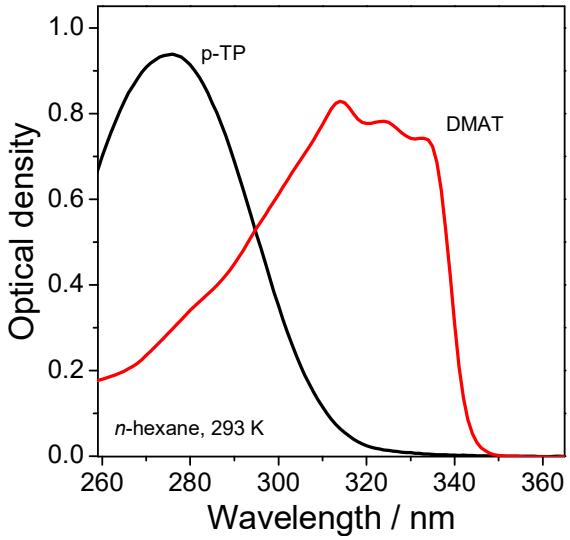

Figure S16. Optical density of 0.03 mM solutions of *para*-terphenyl (*p*-TP) or *para*-N,N-dimethylamino-diphenylacetylene (DMAT) in *n*-hexane. The edge of absorption spectrum is roughly estimated as 325 nm for *p*-TP and 350 nm for DMAT. Spectra were obtained using Edinburgh Instruments F900 Fluorescence Spectrometer.

Table S3. The calculated values of energy gain, E_a and E_v, released in an adiabatic and vertical processes, respectively, in the recombination reactions (1) and (2) for *p*-TP and DMAT solutions in EC, PC, DMC, and DEC (GAMESS, DFT, CAMB3LYP/6-31+G*, PCM)

Reaction	E_a/eV	E_v/eV	Reaction	E_a/eV	E_v/eV
$EC^{+\bullet} + DMAT^{-\bullet}$	6.9	6.1	$EC^{+\bullet} + p\text{-}TP^{-\bullet}$	6.8	6.0
$(EC)_2^{+\bullet} + DMAT^{-\bullet}$	6.2	4.0	$(EC)_2^{+\bullet} + p\text{-}TP^{-\bullet}$	6.1	3.9
$(EC)_3^{+\bullet} + DMAT^{-\bullet}$	6.2	4.0	$(EC)_3^{+\bullet} + p\text{-}TP^{-\bullet}$	6.1	3.9
$EC^{-\bullet} + DMAT^{+\bullet}$	3.6	1.8	$EC^{-\bullet} + p\text{-}TP^{+\bullet}$	4.5	2.6
$(EC)_2^{-\bullet} + DMAT^{+\bullet}$	3.7	1.7	$(EC)_2^{-\bullet} + p\text{-}TP^{+\bullet}$	4.6	2.5
$PC^{+\bullet} + DMAT^{-\bullet}$	6.9	6.0	$PC^{+\bullet} + p\text{-}TP^{-\bullet}$	6.7	5.9
$(PC)_2^{+\bullet} + DMAT^{-\bullet}$	6.2	4.0	$(PC)_2^{+\bullet} + p\text{-}TP^{-\bullet}$	6.1	3.9
$(PC)_3^{+\bullet} + DMAT^{-\bullet}$	6.2	3.9	$(PC)_3^{+\bullet} + p\text{-}TP^{-\bullet}$	6.1	3.8
$PC^{-\bullet} + DMAT^{+\bullet}$	3.7	1.8	$PC^{-\bullet} + p\text{-}TP^{+\bullet}$	4.6	2.6
$(PC)_2^{-\bullet} + DMAT^{+\bullet}$	3.7	1.8	$(PC)_2^{-\bullet} + p\text{-}TP^{+\bullet}$	4.6	2.6
$DMC^{+\bullet} + DMAT^{-\bullet}$	8.3	7.5	$DMC^{+\bullet} + p\text{-}TP^{-\bullet}$	8.2	7.3
$(DMC)_2^{+\bullet} + DMAT^{-\bullet}$	7.8	5.9	$(DMC)_2^{+\bullet} + p\text{-}TP^{-\bullet}$	7.6	5.7
$*(DMC)_2^{+\bullet} + DMAT^{-\bullet}$	7.3	4.9	$*(DMC)_2^{+\bullet} + p\text{-}TP^{-\bullet}$	7.1	4.8
$(DMC)_3^{+\bullet} + DMAT^{-\bullet}$	7.7	5.5	$(DMC)_3^{+\bullet} + p\text{-}TP^{-\bullet}$	7.5	5.4
$DMC^{-\bullet} + DMAT^{+\bullet}$	5.7	3.7	$DMC^{-\bullet} + p\text{-}TP^{+\bullet}$	6.5	4.5
$(DMC)_2^{-\bullet} + DMAT^{+\bullet}$	5.5	3.5	$(DMC)_2^{-\bullet} + p\text{-}TP^{+\bullet}$	6.3	4.3
$(DMC)_3^{-\bullet} + DMAT^{+\bullet}$	5.7	3.6	$(DMC)_3^{-\bullet} + p\text{-}TP^{+\bullet}$	-	4.4
$DEC^{+\bullet} + DMAT^{-\bullet}$	8.1	7.1	$DEC^{+\bullet} + p\text{-}TP^{-\bullet}$	8.0	6.9
$(DEC)_2^{+\bullet} + DMAT^{-\bullet}$	7.1	6.7	$(DEC)_2^{+\bullet} + p\text{-}TP^{-\bullet}$	6.9	4.6
$(DEC)_3^{+\bullet} + DMAT^{-\bullet}$	-	7.1	$(DEC)_3^{+\bullet} + p\text{-}TP^{-\bullet}$	-	-
$DEC^{-\bullet} + DMAT^{+\bullet}$	5.6	3.7	$DEC^{-\bullet} + p\text{-}TP^{+\bullet}$	6.5	4.5
$(DEC)_2^{-\bullet} + DMAT^{+\bullet}$	5.7	5.5	$(DEC)_2^{-\bullet} + p\text{-}TP^{+\bullet}$	6.6	6.3
$(DEC)_3^{-\bullet} + DMAT^{+\bullet}$	5.6	3.5	$(DEC)_3^{-\bullet} + p\text{-}TP^{+\bullet}$	-	4.5

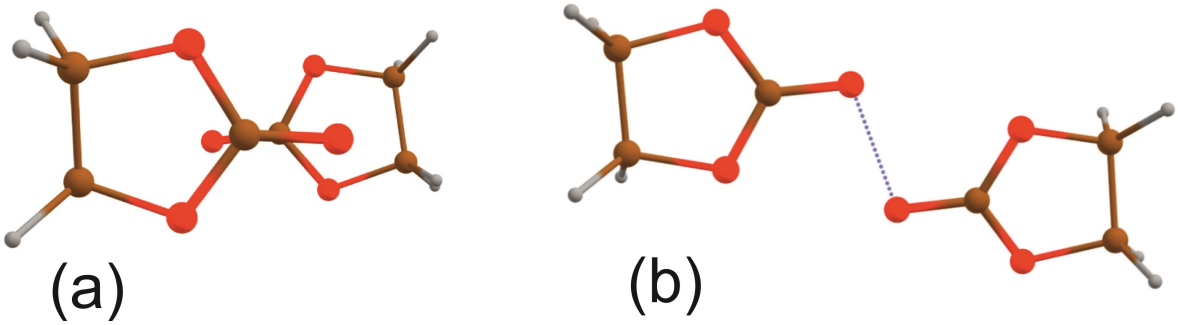

Figure S17. Optimized geometries of $(EC)_2$ (a) and $(EC)_2^{+\bullet}$ (b) (GAMESS, DFT, CAMB3LYP/6-31+G*, PCM).

References to Section S2

4. A. Berndt, M. T. Jones, M. Lehnig, L. Lunazzi, G. Placucci, H. B. Stegmann and K. B. Ulmschneider, *Landolt-Bőrnstein. Numerical data and functional relationships in science and technology. Organic anion radicals; New Series*, Subvolume 9d1; Springer-Verlag: Berlin, Germany, 1980.

5. V. I. Borovkov and L. N. Shchegoleva. Magnetic resonance characteristics of negative polarons in neat poly(3-hexyl-thiophene). *J. Phys. Chem. C* 2019, **123**, 28058−28065 (Supporting Materials).

6. V. I. Borovkov, Do primary carriers of both positive charge and unpaired electron spin exist in irradiated propylene carbonate? *Phys. Chem. Chem. Phys*., *2017*, **19**, 49-53.

7. J. Murakami, K. Okuyama and M. Ito, Multiphoton ionization spectrum of *p*-terphenyl in a supersonic free jet. *Bull Chem. Soc. Jpn*. 1982, **55**, 3422–3423.

8. J. L. Courtneidge, A. G. Davies and D. C. McGuchan, The electron spin resonance spectra of the radical cations of *p*-terphenyl, triphenylene and triptycene. *Recl. Trav. Chim. Pays-Bas*. 1988, **107**, 190−196.